Observation of Nonlinear Effects in Ocean Surface Wave Frequency Spectra

TETSU HARA AND ANDREY V. KARACHINTSEV

Graduate School of Oceanography, University of Rhode Island, Narragansett, Rhode Island

(Manuscript received 31 January 2002, in final form 19 August 2002)

ABSTRACT

Nonlinearity and directionality of an evolving open-ocean surface wave field are investigated under increasing wind forcing. In addition to the frequency wave elevation spectrum, the frequency wave slope spectrum, the bicoherence of the wave elevation time series, and the peak wavenumber at a given frequency estimated by the maximum likelihood method are examined. As the wave field matures, an increasing portion of the high-frequency components of the wave elevation spectrum becomes phase correlated with the dominant wave component. This observation clearly suggests that the contribution to the frequency spectrum from the higher harmonics generated by steep dominant waves becomes increasingly important relative to the contribution from free waves that propagate at their own phase speed predicted by the dispersion relation. The observation therefore invalidates the common assumption that an ocean surface wave spectrum is a superposition of linear surface wave components of different frequencies. In addition, close examination of the frequency slope spectra and the peak wavenumber estimates suggests that the observed phase-coupled modes are generated by short-crested two-dimensional dominant wave patterns rather than by long-crested dominant waves.

1. Introduction

Ocean surface wave fields are commonly characterized by wave elevation frequency spectra or directional wave elevation frequency spectra. A basic assumption behind such spectral representation is that the ocean surface wave field is a superposition of linear surface wave components of different frequencies. Frequency spectra are often converted to wavenumber spectra using an assumption that each spectral component propagates independently at its own phase speed predicted by the theoretical dispersion relation. However, such conversion is not necessarily valid at higher frequencies because of two reasons. One reason is that shorter waves are advected by the orbital velocity of much longer waves. Hence, the observed frequency of shorter waves may be significantly Doppler shifted from its intrinsic frequency determined by the dispersion relation. The other (potentially more serious) reason is that the high-frequency part of the frequency wave elevation spectrum may be dominated by the higher harmonics generated by steep dominant waves and may not contain any information about shorter, freely propagating waves.

It has been observed for some time that the high-frequency part of a wave elevation frequency spectrum is often completely dominated by the bound harmonics of steep dominant waves in laboratory settings (e.g., Mitsuyasu et al. 1979; Hara et al. 1997). Nevertheless, it has been assumed that such a condition does not occur in the open ocean because the peak of the spectrum is usually wider and less pronounced when compared with that in laboratory wind waves (e.g., Mitsuyasu et al. 1979). Belcher and Vassilicos (1997) have recently shown that in theory the high-frequency part of a frequency spectrum is determined completely by the harmonics generated by the largest breaking waves if an ocean surface is saturated with breaking wave crests of a wide range of scales and if surface slope is discontinuous at each breaking wave crest. The model predicts that the wavenumber spectrum decays like k^{-4} in the equilibrium range while the frequency spectrum decays like f^{-4} under such conditions, where k is the wavenumber and f is the frequency of waves. This prediction is not consistent with the linear dispersion relation that relates a wavenumber spectrum of k^{-4} dependence to a frequency spectrum of f^{-5} dependence. This is because the f^{-4} dependence is a result of bound harmonics generated by slope discontinuity at breaking crests of dominant waves; the high-frequency part of the spectrum does not contain any information of shorter waves. Note here that power-law dependence of the frequency spectrum is possible only if singularity exists at breaking wave crests. If dominant waves are steep Stokes waves with no singularity, the spectrum of the bound harmonics is expected to decrease exponentially in f.

It is reasonable to assume that conditions considered by Belcher and Vassilicos (1997) may take place only under extremely high winds. It is plausible, however,

Corresponding author address: Dr. Tetsu Hara, Graduate School of Oceanography, University of Rhode Island, Narragansett, RI 02882.
E-mail: thara@uri.edu

© 2003 American Meteorological Society

Unauthenticated | Downloaded 12/06/21 09:24 AM UTC

that intermediate conditions may take place under less extreme (and more commonly observed) winds, for which the contribution to the frequency spectrum from the harmonics of the dominant waves is at least as important as the contribution from freely propagating waves at higher frequencies. Then, a measured frequency spectrum may still differ from a simple superposition of linear wave components.

In this study, we examine wave elevation records obtained using an array of three wave gauges in an unlimited fetch condition under increasing wind speed. We are particularly interested in a possibility that the high-frequency part of the wave elevation spectrum is determined by the higher harmonics of the dominant waves. If such a condition takes place, each high-frequency mode should have a particular phase relationship relative to the dominant frequency mode. Then, it is expected that the bicoherence of any pair of frequency modes becomes nonzero. We therefore estimate the bicoherence of the wave elevation record throughout the wave development. In addition, the frequency wave elevation spectrum and the frequency wave slope spectrum are calculated, and the location of the peak wavenumber is estimated at each frequency using the maximum likelihood method (MLM). These analyses are combined to study how the nonlinearity and directionality of the wave field evolve and how the high-frequency part of the spectrum is increasingly affected by the higher harmonics of dominant waves as the wave field grows.

2. Experiments

The marine boundary layer (MBL) experiment was conducted from the Research Platform *FLIP* (*Floating Instrument Platform*) during 30 days in April–May of 1995 about 60 km west of Monterey, California. The R/P *FLIP* is a 360-foot spar buoy, and its high degree of stability enables precision oceanographic and meteorological measurements to be obtained free of motions associated with conventional ships. In 10-foot seas, *FLIP*'s vertical motion is only a few inches. During the MBL experiment, the *FLIP* was in a three-point mooring in about 2000 m of water. An array of three wave staffs was part of the instrumentation package of the MBL experiment. The distance between the elements of the triangular array was 1 m. A vertical array of sonic and cup anemometers at various levels between 3.95 and 18.1 m above water surface provided information about the wind profile. The subsurface current was measured with an ultrasonic current meter mounted 6 m under the platform's waterline.

The wave staff array, based on a set of 10-m-long capacitance wave gauges, was implemented by the Scripps Institution of Oceanography. The output of the wave staffs was sampled at a rate of 10 Hz. The wave staff calibration was made against the wave elevation measured by the acoustic depth meter. The data used in this study were obtained over three days [yearday (YD) 123–125], during which the wind was blowing from north (between 320° and 340°) and its speed increased from 6 to 13 m s^{-1}. The fetch was effectively unlimited at the experimental site, and the wave field was fully developed toward the end of the 3-day period.

3. Data analysis of wave elevation records

In addition to calculating the conventional frequency spectra, we employed three different signal processing techniques to investigate the directionality and nonlinearity of the wave field.

a. Wave elevation frequency spectrum

The frequency wave elevation spectrum, denoted by $\Psi(f)$, was obtained using a 30-min-long data record, divided into 34 overlapping 102-s-long segments, using the Hann window and the fast Fourier transform.

b. Wave slope frequency spectrum

Using the output from the triangular array of the wave gauges, we obtained the time series of the two (along-wind and crosswind) components of the surface slope. The results were then used to calculate the frequency spectra, denoted by $S(f)$, of the two components of the surface slope. Because the spacing between the wave gauges was 1 m, the calculated wave slope included contributions from waves much longer than 1 m. The wave length, 1 m, corresponds to wavenumber $k = 6.3$ rad m^{-1} and frequency $f = 1.25$ Hz according to the linear dispersion relation.

c. Peak wavenumber estimation using maximum likelihood method

The maximum likelihood method was employed to estimate the energy distribution in the two-dimensional wavenumber domain at a given frequency. The method was originally developed by Capon et al. (1969), and later an alternative formulation was provided by Davis and Regier (1977). Let us denote the position of the ith wave gauge by $\mathbf{x}_i$ ($i = 1, 2, 3$). The normalized cross power spectrum matrix at an angular frequency ω is formed from the products of the Fourier coefficient of its ith element, denoted by A_i, and the complex conjugate of the Fourier coefficient of its jth element:

$$Q_{ij}(\omega) = \left\langle \frac{A_i(\omega)}{|A_i(\omega)|} \frac{A_j(\omega)^*}{|A_j(\omega)|} \right\rangle, \tag{1}$$

where the asterisk denotes the complex conjugate and angle brackets denote ensemble average. The estimate of the frequency wavenumber spectrum is given as

$$\Psi(\mathbf{k}, \omega) = h\left[\sum_{i=1}^{3}\sum_{j=1}^{3} Q_{ij}^{-1}(\omega) e^{i\mathbf{k}(\mathbf{x}_i - \mathbf{x}_j)}\right]^{-1}, \tag{2}$$

Unauthenticated | Downloaded 12/06/21 09:24 AM UTC

where **k** is a wavenumber vector and h is a scaling constant.

Because the wavenumber spectral estimation is made with only three wave gauges, the result is not accurate enough to resolve the detailed shape of the spectrum. It has been known for some time that the MLM estimation of the wavenumber spectrum usually predicts the correct peak location if the real spectrum contains a single peak. If the real spectrum contains two or more peaks, however, the MLM estimation may or may not resolve the individual peaks. To investigate the MLM performance in detail, we have performed several tests using simulated wave fields of different spectral shapes sampled by the same wave gauge array. It has been found that, when multiple peaks are present and are not far apart from each other, the MLM tends to yield a single peak at a location that is roughly at the center of the overall spectral power distribution. For example, if there are two spectral peaks of comparable magnitude in the real spectrum, the MLM result predicts a single peak halfway between the two real peaks. More details are given in Karachintsev (1998).

Based on these test results, we have decided to use only the information about the location of the spectral peak in the two-dimensional wavenumber domain. In all cases examined using the observed wave data, the MLM results yielded a single peak. The peak wavenumber was always in the mean wind direction but its magnitude varied considerably from case to case as shown in section 4.

d. Bispectral analysis

Over the last two decades, bispectral analysis has been used by several investigators for studying nonlinear effects in oceanic surface gravity waves. The method is typically applied to wave fields for which strong nonlinear coupling is expected. In particular, bispectral analysis made it possible to follow the development of nonlinear interactions in gravity wave trains shoaling on a sloping bottom (e.g., Elgar and Guza 1985). The bispectra were also examined for deep-water gravity waves in the vicinity of the spectral peak in a wind–wave tank (Masuda and Kuo 1981). Because it has been assumed that nonlinear coupling is less pronounced in open-ocean waves than in shoaling waves or in laboratory waves, no bispectral analyses have been performed for open-ocean deep-water waves. Yet, we present in this study that the bispectral analysis can be used effectively in combination with the MLM analysis to address nonlinearity of the open-ocean wave fields that are strongly forced by wind.

The bispectrum B of any discrete time series is defined as

$$B(\omega_1, \omega_2) = \langle A(\omega_1)A(\omega_2)A^*(\omega_1 + \omega_2)\rangle, \qquad (3)$$

where A is the Fourier coefficient. If the wave field is linear and the phase relationship among individual sinusoidal components is random, the value of the bispectrum is zero provided the number of realizations, or degrees of freedom (d.o.f.), in averaging is sufficiently large. However, as the wave field becomes nonlinear, phase-coupled modes appear and give rise to nonzero bispectral values. To examine this nonlinearity effect, it is more convenient to use the bicoherence b, defined as

$$b(\omega_1, \omega_2) = \left[\frac{|B(\omega_1, \omega_2)|^2}{\langle|A(\omega_1)A(\omega_2)|^2\rangle\langle|A(\omega_1 + \omega_2)|^2\rangle}\right]^{1/2}. \qquad (4)$$

This particular normalization constrains the bicoherence values to range from 0 to 1, thus making it similar to the one-dimensional coherence function.

Because of the symmetry properties of the bispectrum and bicoherence, these quantities can be uniquely described by their values in a bifrequency octant. For a digital time series sampled with a frequency $2\omega_N$ where ω_N is the Nyquist frequency, it is sufficient to define the bicoherence in a triangle in (ω_1, ω_2) space with vertices at $(\omega_1 = \omega_2 = 0)$, $(\omega_1 = \omega_2 = \omega_N/2)$ and $(\omega_1 = \omega_N/2, \omega_2 = 0)$.

Even for a truly linear random wave field, the value of the bicoherence estimate may be different from zero if the time series has a finite length. The accuracy of the bispectral analysis is strongly dependent on the number of degrees of freedom used in averaging. Therefore, the time series used for bicoherence estimation should be long enough to allow for a sufficiently large number of degrees of freedom in order to detect a nonzero bicoherence level with confidence. Haubrich (1965) proposed the following expression for estimating a 95% significance level of zero bicoherence:

$$b^2_{95\%} < 6/\text{d.o.f.}; \qquad (5)$$

that is, there is only a 5% or less chance that a bicoherence estimate squared exceeds this value if the process is truly Gaussian. Elgar and Guza (1985) point out that according to numerical simulations the actual values of the 95% significance level are about 1/4 of the value given by Eq. (5). Therefore, Eq. (5) can be readily used if one wants to obtain a conservative estimate of 95% significance levels.

The number of degrees of freedom was calculated as follows. A 1-h-long wave elevation time series was subdivided into 175 short records, each 205 points long. A Hann window with 50% overlap was applied to each short time series to reduce spectral leakage, and higher-order spectra from each of the 175 records were ensemble averaged, producing estimates with about 350 degrees of freedom and a final frequency resolution of 0.049 Hz. Then, Eq. (5) gives a minimum detection value of about 0.13, that is, nonzero bicoherence values can be detected with 95% confidence if the observed bicoherence value exceeds 0.13. We therefore report the bicoherence estimates only if they exceed this threshold. We do not report the estimated values of the bispectrum,

Unauthenticated | Downloaded 12/06/21 09:24 AM UTC

TABLE 1. Conditions during the experiment.

YD	Wind speed (m s^{-1})	Wind direction (°)	Mean current (m s^{-1})	Current direction (°)
123.29	6.6	320	0.23	3
124.63	9.2	335	0.20	335
125.24	12.5	328	0.23	310

because it is difficult to obtain statistically reliable estimates with the limited amount of data available.

4. Results

The time series from the MBL experiment covered a period of steadily increasing wind and growing wind seas under an unlimited fetch condition. The wind and current data are summarized in Table 1 for three selected periods. The 10-m wind speed U_{10} increased from 6.6 m s^{-1} at YD 123.29 to 12.5 m s^{-1} at YD 125.24 while the wind direction changed little over the period.

We first present the wave elevation frequency spectra at the three periods in Fig. 1. Dotted and dashed lines are added in the figure to indicate f^{-4} and f^{-5} dependence of the spectrum, respectively. At YD 123.29, two swell systems (peak frequencies at 0.095 and 0.15 Hz) are present as well as a local wind sea with its peak frequency of 0.27 Hz. The wave age c_p/U_{10} is 0.90 if the peak phase speed c_p is evaluated at the peak of the local wind sea. The wind sea part of the spectrum appears to follow the f^{-5} dependence.

By YD 124.63 one of the swell systems merges with the wind sea with its peak frequency of 0.14 Hz. A separate swell system with its peak frequency of 0.085 Hz is observed. The wave age increases to 1.23, suggesting that the wind sea is fully developed. The spectrum just above the peak frequency (roughly below 0.3 Hz) follows the f^{-4} dependence; the high-frequency part is closer to the f^{-5} dependence. Notice that the spectral level at higher frequencies has increased by almost one order of magnitude from YD 123.29.

At YD 125.24, the wind sea and the swell system merge and a single spectral peak at 0.115 Hz is observed. The wave age is now 1.09. The low-frequency part is closer to the f^{-4} dependence, and the high-frequency part decreases like f^{-5} or slightly faster. The

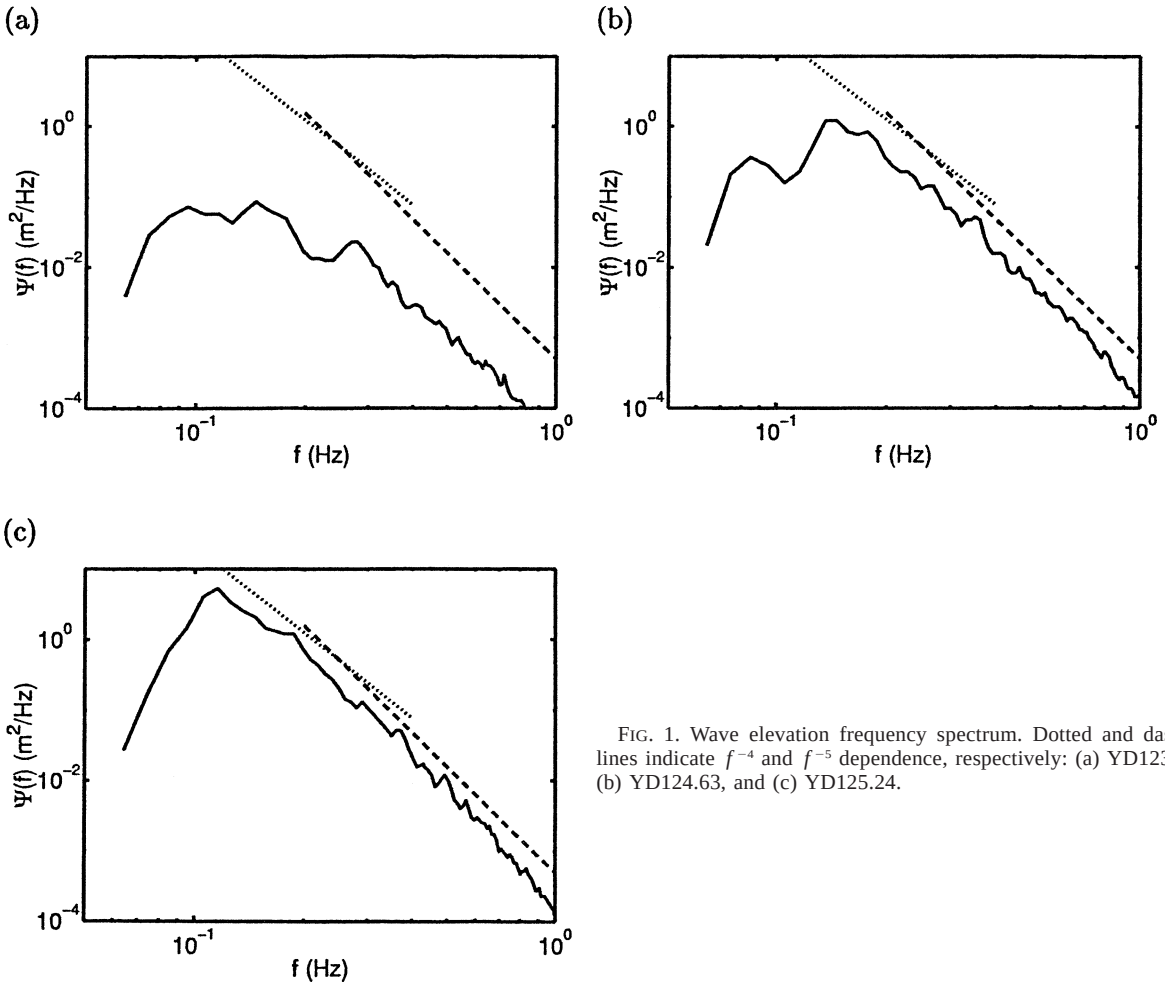

FIG. 1. Wave elevation frequency spectrum. Dotted and dashed lines indicate f^{-4} and f^{-5} dependence, respectively: (a) YD123.29, (b) YD124.63, and (c) YD125.24.

Unauthenticated | Downloaded 12/06/21 09:24 AM UTC

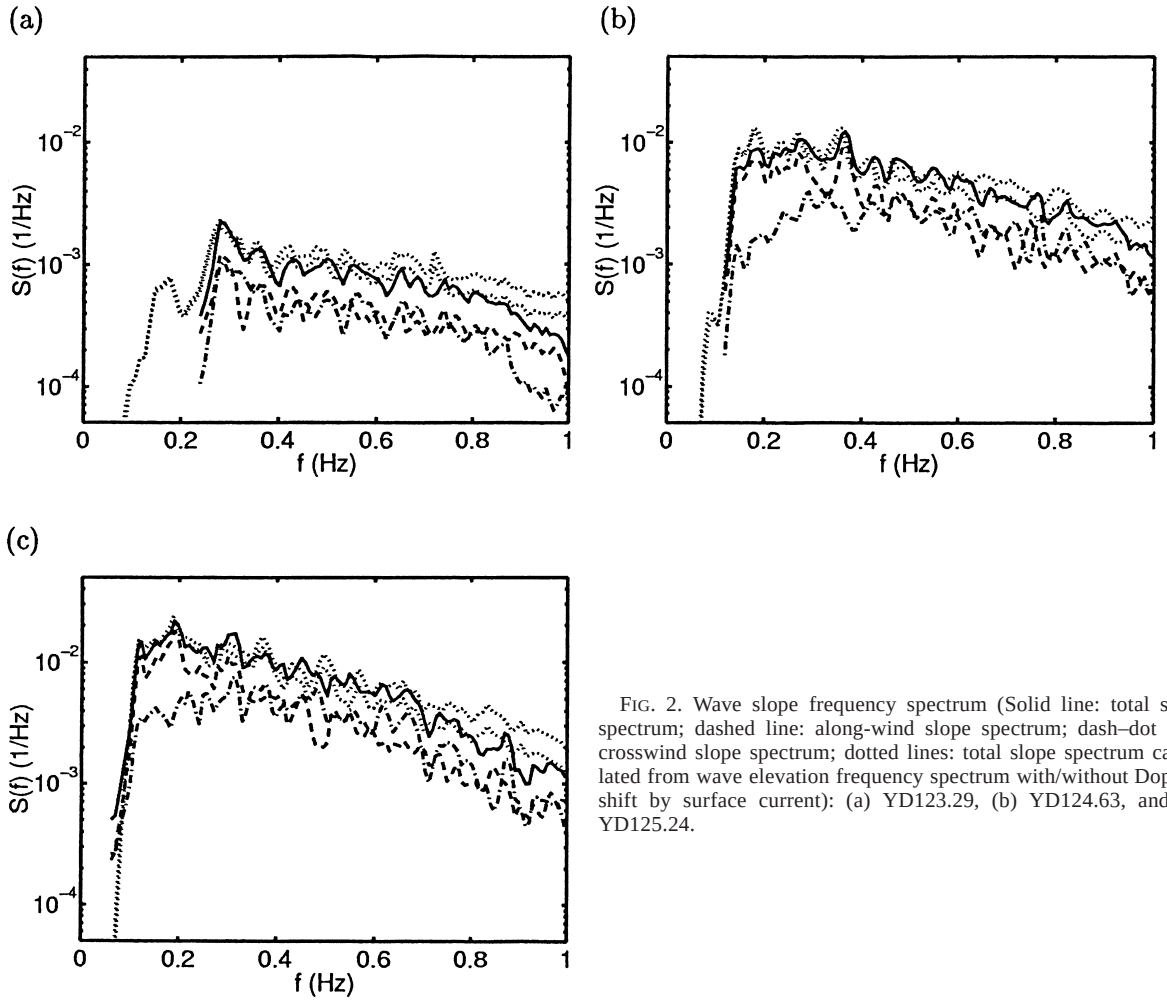

FIG. 2. Wave slope frequency spectrum (Solid line: total slope spectrum; dashed line: along-wind slope spectrum; dash–dot line: crosswind slope spectrum; dotted lines: total slope spectrum calculated from wave elevation frequency spectrum with/without Doppler shift by surface current): (a) YD123.29, (b) YD124.63, and (c) YD125.24.

spectral level at higher frequencies is only slightly increased from YD 124.63.

Let us now examine the bicoherence, the slope spectrum, and the MLM peak wavenumber estimates. At YD 123.29, the bicoherence values are always below the minimum detection value of 0.13 and are not presented. This result suggests that there is no significant phase coupling among different frequency components. The wind sea part of the slope spectrum is shown in Fig. 2a. The slope spectrum of the swell part cannot be calculated accurately because of the low signal level and is not shown. It is seen that the along-wind and crosswind components are almost comparable in magnitude throughout the wind sea part of the spectrum, except above 0.9 Hz. Therefore, the directional spreading must be significantly broad. The MLM result in Fig. 3a shows that the predicted peak wavenumber over the range of 0.3–0.9 Hz is roughly 70%–80% of the theoretical dispersion relation including the Doppler shift by surface current. This deviation from the dispersion relation is likely due to the directional spreading of the spectrum as explained in the next section.

As the wave field develops, the bicoherence values begin to exceed the minimum detection threshold as shown in Fig. 4. At YD 124.63, the peak frequency component at 0.14 Hz shows phase coupling with some of the higher-frequency components. At YD 125.24, the coupling between the peak frequency component at 0.115 Hz and high-frequency components (above 0.4 Hz) is persistent and stronger, with bicoherence values as high as 0.2. These results clearly suggest that part of the high-frequency components represents waves that are bound to and propagate with the dominant frequency component rather than free waves propagating at their own phase speed. (We cannot attribute the observed nonzero bicoherence to resonant wave interactions, because there are no three-wave interactions of deep-water surface gravity waves!) The slope spectra in Figs. 2b and 2c show much lower levels of crosswind slope components near the spectral peak. Thus, waves near the wind sea peak are mostly propagating in the wind direction. However, the high-frequency parts (above 0.4 Hz in Fig. 2b and above 0.3 Hz in Fig. 2c) show comparable magnitudes of along-wind and crosswind slope

Unauthenticated | Downloaded 12/06/21 09:24 AM UTC

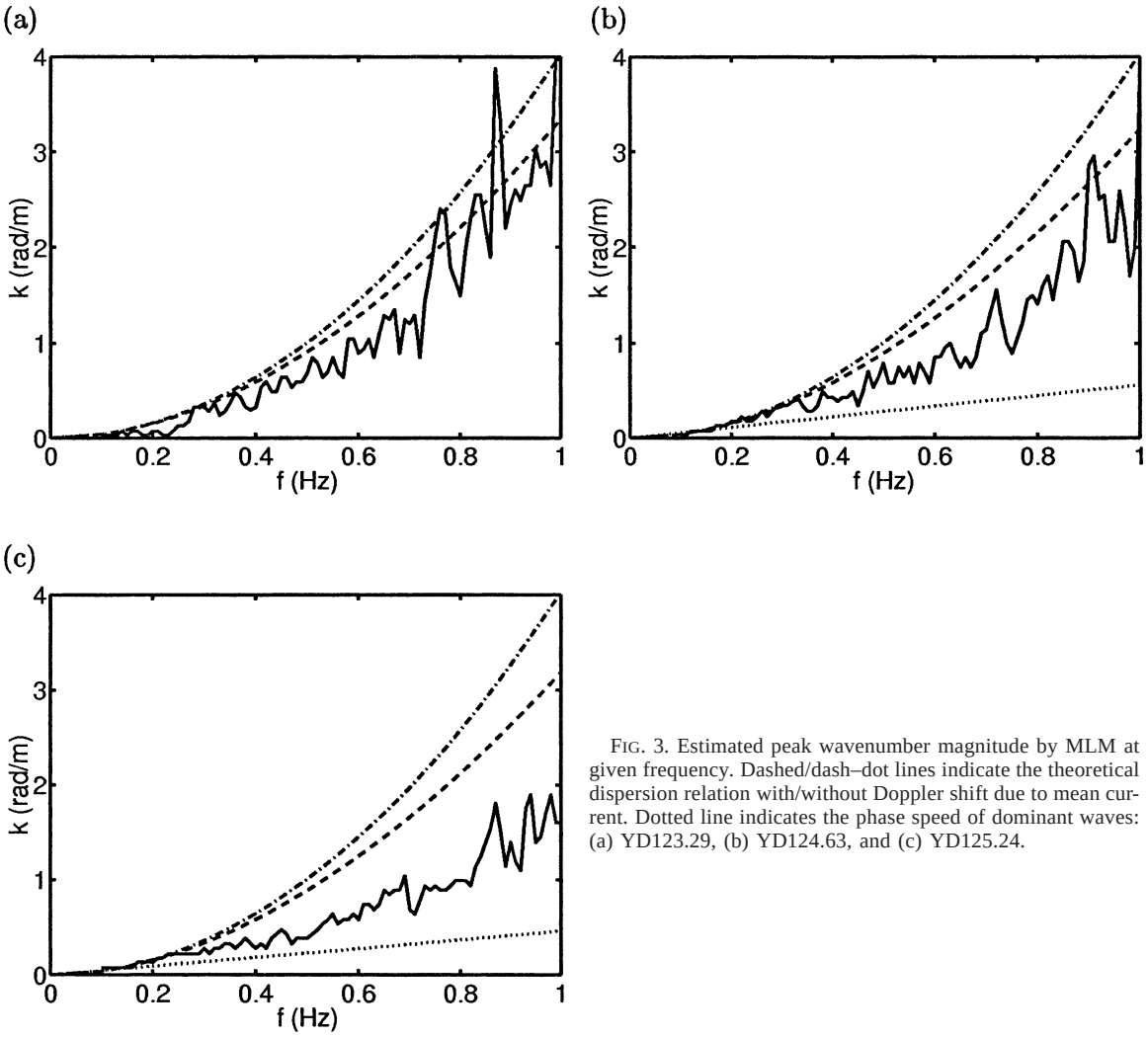

FIG. 3. Estimated peak wavenumber magnitude by MLM at given frequency. Dashed/dash–dot lines indicate the theoretical dispersion relation with/without Doppler shift due to mean current. Dotted line indicates the phase speed of dominant waves: (a) YD123.29, (b) YD124.63, and (c) YD125.24.

components. The predicted peak wavenumber magnitude, shown in Figs. 3b and 3c, is consistent with the theoretical dispersion relation near the wind sea peak but is much smaller at higher frequencies (about 60%–80% in Fig. 3b and about 50%–60% in Fig. 3c) at which the phase coupling with the dominant frequency mode is observed.

5. Discussion

In the previous section, we have shown that the high-frequency components of the wave elevation spectrum become increasingly phase coupled to the dominant frequency component as the wave field evolves. This observation strongly suggests that the high-frequency part of the spectrum becomes progressively dominated by the bound harmonics of the dominant waves. This is an important result because it clearly invalidates the common assumption that an ocean surface wave elevation spectrum is a superposition of linear surface wave components of different frequencies.

We have also observed that, as the wave field develops, the estimated peak wavenumber magnitude slowly decreases over the frequency range at which the phase coupling is observed. The slope spectra of along-wind and crosswind components remain comparable away from the spectral peak throughout the wave field evolution, suggesting that the bound harmonics of the dominant waves are not all aligned with wind.

In this section, we attempt to combine all the observations in the previous section to construct a more complete picture of how the wave field develops. To be specific, we estimate the evolution of the full three-dimensional frequency–wavenumber spectrum of the wave field—that is, we estimate how the energy is distributed in the two-dimensional wavenumber domain at a given frequency. This exercise helps to distinguish the free-wave modes and the phase-coupled modes at any given frequency, because they occupy different parts of the wavenumber spectrum.

At YD 123.29, no significant nonlinear coupling is observed. Therefore, all wave components are expected

Unauthenticated | Downloaded 12/06/21 09:24 AM UTC

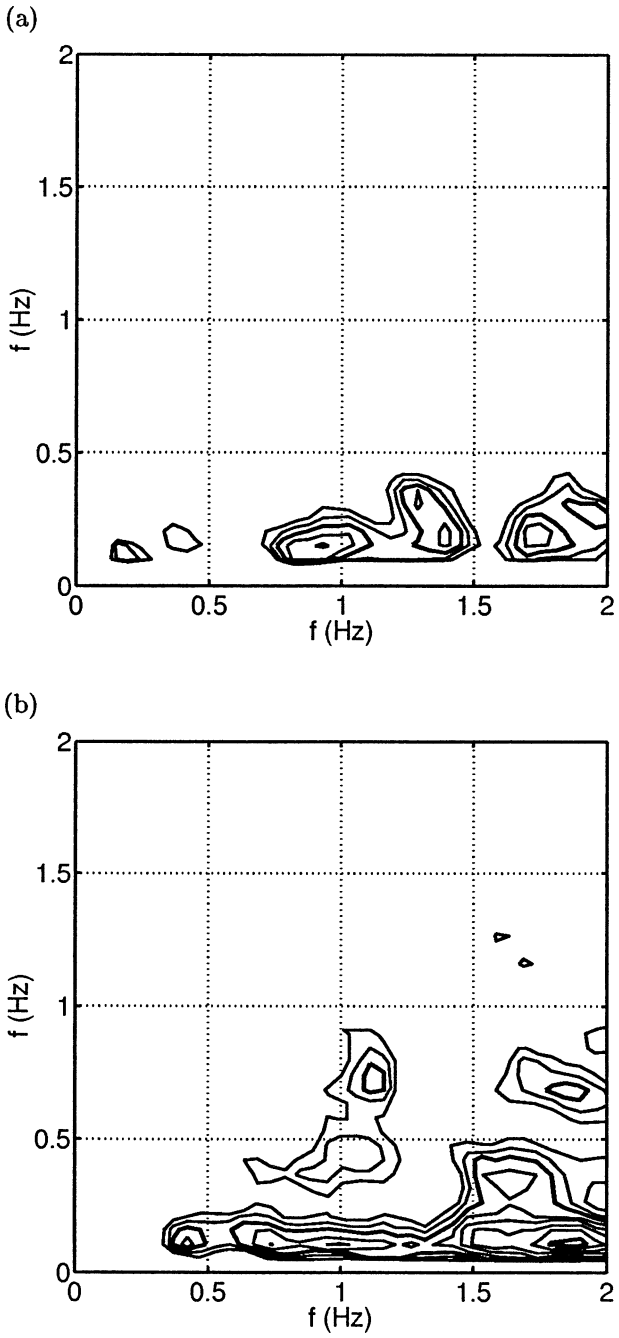

FIG. 4. Contour plots of bicoherence of wave elevation time series. The contour levels are every 0.01 starting from 0.13. The thicker contours are at 0.15 and 0.2: (a) YD124.63 and (b) YD125.24.

to be linear and to propagate freely at the speed predicted by the dispersion relation. Furthermore, it is observed that along-wind and crosswind slope spectra are comparable over the wind sea part of the spectrum. For a given frequency, we may consider two simple examples of wavenumber spectra that consist of free waves only and yield comparable levels of along-wind and crosswind slope spectra as shown in Figs. 5a and 5b. Here, we have chosen a frequency of 0.5 Hz for demonstration purposes and have neglected the Doppler shift by the surface current for simplicity. The wind direction is defined to be in the x direction. The first example consists of two wave fields propagating in $\pm 45°$ relative to the wind direction. In the second example, the wave energy is spread uniformly between $\pm 90°$ relative to the wind direction. In both cases the MLM would predict the peak wavenumber that is in the wind direction but whose magnitude is less than the value predicted by the dispersion relation, as indicated by crosses in the figures. This is because the MLM tends to predict the peak wavenumber location that is in the center of the overall spectral distribution in the two-dimensional wavenumber domain (Karachintsev 1998). In the first example, the magnitude of the peak wavenumber would be about 71% of the value predicted by the dispersion relation; the prediction in the second example would be at about 64%. These results are somewhat modified in the presence of Doppler shift by a surface current. Nevertheless, the locations of the peak wavenumber in these examples are roughly consistent with the MLM estimates of the peak wavenumber at YD 123.29 shown in Fig. 3a.

If a wave mode at a particular frequency f is phase coupled to the dominant frequency mode that propagates in the wind direction, its propagation speed must have an along-wind component that is identical to the phase speed of the dominant waves. A trivial example is the bound higher harmonics of steep long-crested waves. In addition, it is possible that the phase-coupled mode results from the directional higher harmonics of steep short-crested waves (e.g., a crescent-shape wave pattern), whose topography is two-dimensional but is preserved as it propagates downwind. Let us express such a phase-coupled mode as

$$e^{i(k_x x + k_y y - 2\pi f t)}, \tag{6}$$

with

$$k_x = k\cos\theta, \qquad k_y = k\sin\theta, \tag{7}$$

where θ is the direction of the phase-coupled mode relative to the wind direction. Then, it must satisfy that

$$\frac{2\pi f}{k_x} = c_p \quad \text{or} \quad k_x = \frac{2\pi f}{c_p}, \tag{8}$$

where c_p is the phase speed of the dominant waves. If this condition is shown graphically, the wave energy of the phase-coupled modes must be distributed along the solid line in Fig. 5c, where c_p has been chosen to be 13.4 m s^{-1}, corresponding to the peak frequency of 0.115 Hz in this particular example.

Because the phase coupling between the dominant wave mode and high-frequency wave modes strengthen as the wave field develops from YD 124.63 to YD 125.24, it is expected that an increasing proportion of the wave energy is distributed somewhere along the solid line in Fig. 5c rather than in the free-wave location shown in Figs. 5a or 5b. Then, it is expected that the MLM estimate of the peak wavenumber moves from

Unauthenticated | Downloaded 12/06/21 09:24 AM UTC

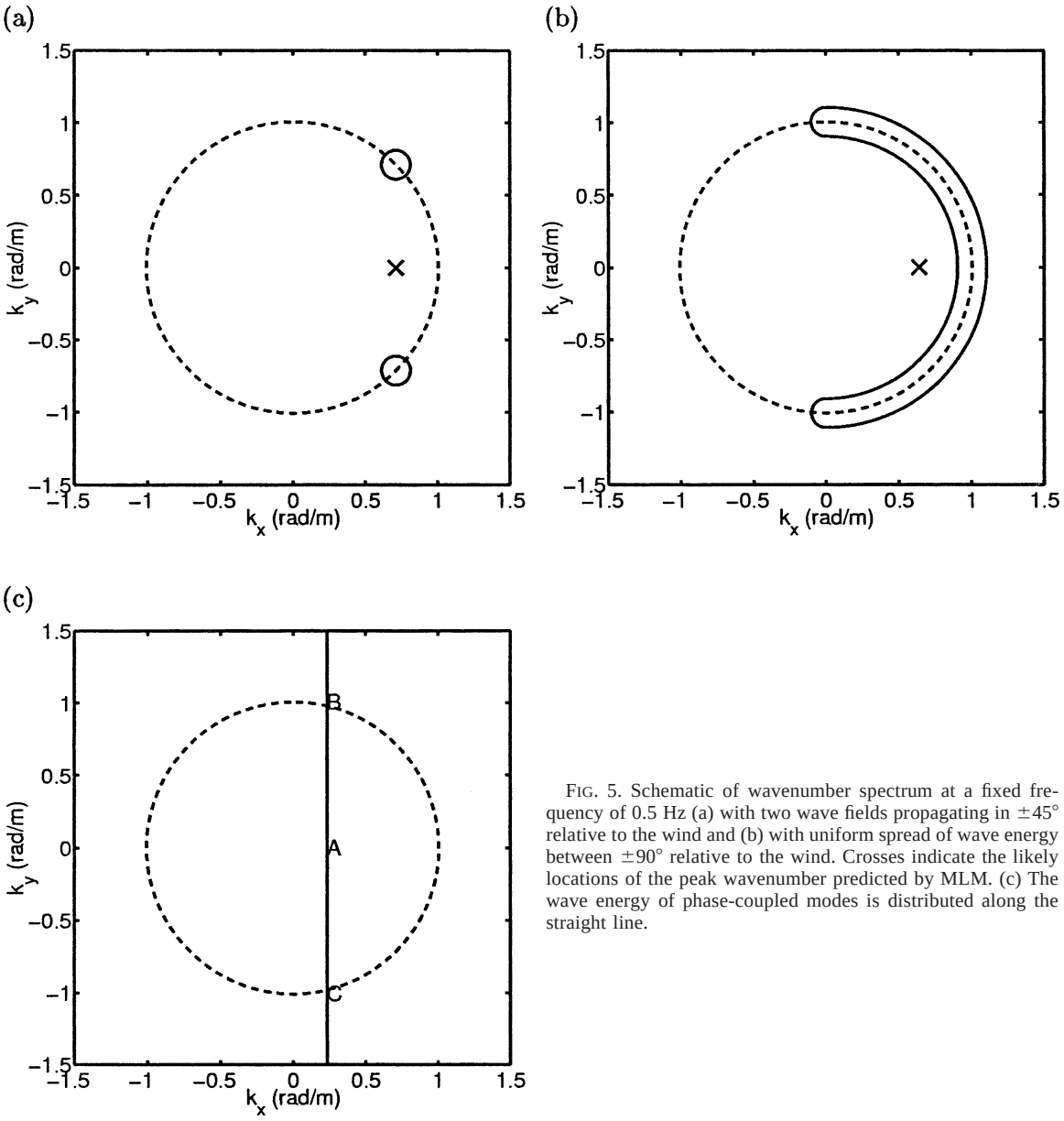

FIG. 5. Schematic of wavenumber spectrum at a fixed frequency of 0.5 Hz (a) with two wave fields propagating in ±45° relative to the wind and (b) with uniform spread of wave energy between ±90° relative to the wind. Crosses indicate the likely locations of the peak wavenumber predicted by MLM. (c) The wave energy of phase-coupled modes is distributed along the straight line.

the cross in Figs. 5a or 5b toward point A in Fig. 5c, as the wave field evolves. Such a trend is indeed observed in Figs. 3b and 3c, where the estimated peak wavenumber magnitude gradually decreases and approaches the phase speed of the dominant waves (dotted lines) over the frequency range in which the phase coupling is present.

The remaining question is the directionality of the phase-coupled mode—that is, whether the wave energy of the phase-coupled mode comes from the bound higher harmonics of long-crested dominant waves or from the directional higher harmonics of short-crested dominant waves. In the former case, the energy must be concentrated near point A in Fig. 5c, whereas the energy may be distributed anywhere along the straight line in Fig. 5c in the latter case. This question can be partially answered by investigating the wave slope spectrum. On one hand, if most of the phase-coupled mode is concentrated near point A, its contribution to the total slope spectrum must be much smaller than the contribution from the free-wave modes, because the contribution to the slope spectrum is equal to the elevation spectrum multiplied by the square of the wavenumber magnitude. On the other hand, if the energy is concentrated near points B and C, where the phase-coupled mode happens to satisfy the dispersion relation, its contribution to the slope spectrum is comparable to that of the free-wave modes.

In Fig. 2, the dotted lines indicate total frequency slope spectra calculated from the frequency elevation

Unauthenticated | Downloaded 12/06/21 09:24 AM UTC

spectra multiplied by the square of the wavenumber with an assumption that all wave are propagating at their phase speeds predicted by the dispersion relation. The higher spectral values are obtained using the wavenumber without the Doppler shift (dash–dot line in Fig. 3); the lower values are calculated using the wavenumber with the Doppler shift included (dashed line in Fig. 3). The true slope spectrum should be somewhere between the two dotted lines in Fig. 2 if all waves are indeed propagating at their own phase speeds. It is observed that the measured total slope spectrum is roughly consistent with the slope spectrum calculated from the wave elevation spectrum up to about 0.8 Hz throughout the wave evolution. This observation implies that majority of the wave energy of the phase-coupled modes is distributed near points B and C rather than near point A and contributes to the slope spectrum in the same manner as the free-wave modes. Hence, the phase-coupled modes are likely to be strongly directional and result from the higher harmonics of short-crested (two dimensional) dominant wave patterns. This final part of the discussion is based on many speculations and is far from conclusive. It is highly desirable to obtain further observational data, ideally in the form of directly observed three-dimensional frequency–wavenumber spectra, so that the directionality of the phase-coupled modes is fully examined.

6. Concluding remarks

We have examined how nonlinearity and directionality influence the frequency spectrum of a growing wave field under increasing wind forcing. In an early stage of the wind sea development, freely propagating waves with significant directional spreading dominate the frequency spectrum. As the wave field develops, we observe increasing contribution to the high-frequency part of the spectrum from the higher bound harmonics of steep dominant waves. This observation clearly invalidates the common assumption that an ocean surface wave frequency spectrum is a superposition of linear surface wave components.

The combined analysis of the MLM and the slope spectrum suggests that the phase-coupled modes result from the directional higher harmonics of short-crested (two dimensional) dominant wave pattern rather than from the bound harmonics of long-crested dominant waves. This aspect requires further confirmation in future studies.

Although our observations show qualitative tendency toward the model prediction by Belcher and Vassilicos (1997) that the frequency spectrum of a wind sea is determined by the bound harmonics of sharp-crested dominant waves, there are quantitative differences. Their model predicts that discontinuity in the slope at sharp breaking crests produces a frequency spectrum that is proportional to f^{-4} at high frequencies. However, our observed frequency spectrum is proportional to f^{-5} or slightly steeper. It is straightforward to extend the argument by Belcher and Vassilicos (1997) that, if the curvature of the surface elevation is discontinuous at breaking crests, the frequency spectrum should be proportional to f^{-6} at high frequencies. Therefore, it is feasible that our observed phase-coupled modes may result from breaking wave crests where singularity is somewhere between slope discontinuity and curvature discontinuity.

Acknowledgments. We thank Drs. James Edson and Jeffrey Hare and Mr. Lloyd Green for providing the experimental data. We also acknowledge helpful comments from Drs. Jerome Smith and Stephen Belcher during this study. The work was supported by the Office of Naval Research through Grant N00014-96-10542.

REFERENCES

Belcher, S. E., and J. C. Vassilicos, 1997: Breaking waves and the equilibrium range of wind-wave spectra. *J. Fluid Mech.,* **342,** 377–401.

Capon, J., R. J. Greenfield, and R. J. Kolker, 1969: Multidimensional maximum-likelihood processing of a large aperture seismic array. *Proc. IEEE,* **55,** 192–211.

Davis, R. E., and L. A. Regier, 1977: Methods for estimating directional wave spectra from multi-element arrays. *J. Mar. Res.,* **35,** 453–477.

Elgar, S., and R. T. Guza, 1985: Observation of bispectra of shoaling surface gravity waves. *J. Fluid Mech.,* **161,** 425–448.

Hara, T., E. J. Bock, and M. Donelan, 1997: Frequency–wavenumber spectrum of wind-generated gravity-capillary waves. *J. Geophys. Res.,* **102,** 1061–1072.

Haubrich, R. A., 1965: Earth noises, 5 to 500 millicycles per second. *J. Geophys. Res.,* **70,** 1415–1427.

Karachintsev, A. V., 1998: Observations of nonlinear wave spectra in open ocean and shallow coastal waters. M.S. thesis, Graduate School of Oceanography, University of Rhode Island, 92 pp.

Masuda, A., and Y. Y. Kuo, 1981: Bispectra for the surface displacement of random gravity waves in deep water. *Deep-Sea Res.,* **28A,** 223–237.

Mitsuyasu, H., Y.-Y. Kuo, and A. Masuda, 1979: On the dispersion relation of random gravity waves. Part 2. An experiment. *J. Fluid Mech.,* **92,** 731–749.

Unauthenticated | Downloaded 12/06/21 09:24 AM UTC